analytical chemistry

Article

pubs.acs.org/ac

Development of a Quasi-Steady Flow Electrochemical Paper-Based Analytical Device

Jaclyn A. Adkins, Eka Noviana, and Charles S. Henry*

Department of Chemistry, Colorado State University, Fort Collins, Colorado 80523, United States

Supporting Information

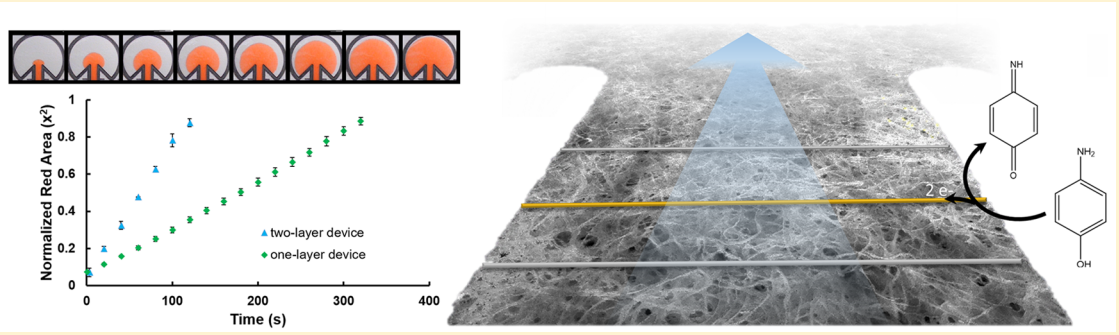

ABSTRACT: An electrochemical paper-based analytical device (ePAD) was developed for quasi-steady flow detection at microwire electrodes, for the first time. The device implements a fan shaped geometry connected to an analysis channel whereby solution is pulled from an inlet, through a channel, and into the steadily increasing capillary network of the fan. The network counteracts the decrease in solution flow rate associated with increasing viscosity within the channel, generating quasi-steady flow within the analysis channel. Microwire electrodes were embedded between two paper layers within the analysis channel, such that solution flow occurred on both sides of the wire electrodes. The quasi-steady flow ePAD increased the current by 2.5 times and 0.7 times from a saturated channel with no flow and from a single-layer paper device with flow, respectively. Amperometric detection was used for flow injection analysis (FIA) of multiple analytes at both Au and Pt microwire working electrodes, both of which provided similar sensitivity (ca. 0.2 mM^{-1}) when normalized to the same standard. The two-layer paper devices provided a detection limit of 31 μM for *p*-aminophenol (PAP) using Pt electrodes and was also used to detect enzyme activity for the reaction of β-galactosidase with *p*-aminophenyl-galactopyranoside (PAPG). Measured enzyme kinetics provided similar V_{max} (0.079 mM/min) and K_m (0.36 mM) values as those found in the literature. This device shows great promise toward use in enzyme-linked immunosorbent assays or other analytical techniques where flow or washing steps are necessary. The developed sensor provides a simple and inexpensive device capable of performing multiple injection analysis with steady-flow and online detection that would normally require an external pump to perform.

The development of microfluidic devices in combination with lab-on-a-chip technologies has offered platforms that are inexpensive, with minimal reagent use, waste generation, and analysis time. Furthermore, they are often simpler to use than traditional benchtop instrumentation.[1] Many microfluidic devices have also been designed with the intention of point-of-need measurements away from the traditional laboratory setting. While many microfluidic devices have been demonstrated in the laboratory, few have been adapted to point-of-need measurements.[2] One reason for this lack of product acceptance is that many devices require external pumps and tubing for continuous flow, making them inconvenient for field measurements. Paper has long been used as a platform for analytical measurements and more recently in microfluidic devices since Whitesides and co-workers published the use of photoresist-patterned filter paper for the multiplexed biomarker detection.[3] Since then, a variety of methods for device fabrication and analyte detection in microfluidic paper-based analytical devices (μPADs) have been developed.[4−6] The popularity of using paper as a substrate for analytical analysis lies in its inherent advantage of being an inexpensive, disposable, and easy to modify platform that contains a capillary network capable of fluid transport and manipulation without the need for external pumps.[7,8] These advantages also make μPADs well suited for point-of-care (POC) and environmental analysis where demand for low-cost and simple to use devices that can contain stored reagents is high.[6,9,10]

While colorimetric detection has been the most common detection method for μPADs due to its simple reactions and easily visible results, electrochemical paper-based analytical devices (ePADs), as first proposed by Dungchai et al.[11] can provide lower detection limits and generate more quantitative results when compared with colorimetric detection.[12] Detection

Received: August 3, 2016
Accepted: September 26, 2016
Published: September 26, 2016

DOI: 10.1021/acs.analchem.6b03010
Anal. Chem. 2016, 88, 10639−10647

Scheme 1. Quasi-Stationary Flow ePAD Fabrication Showing (A) the Device Layers, (B) the Top View of the Device Design (with Packing Tape Back Layer Moved to the Side Slightly for Visualization), and (C) the Device Image with Electrode Leads Attached

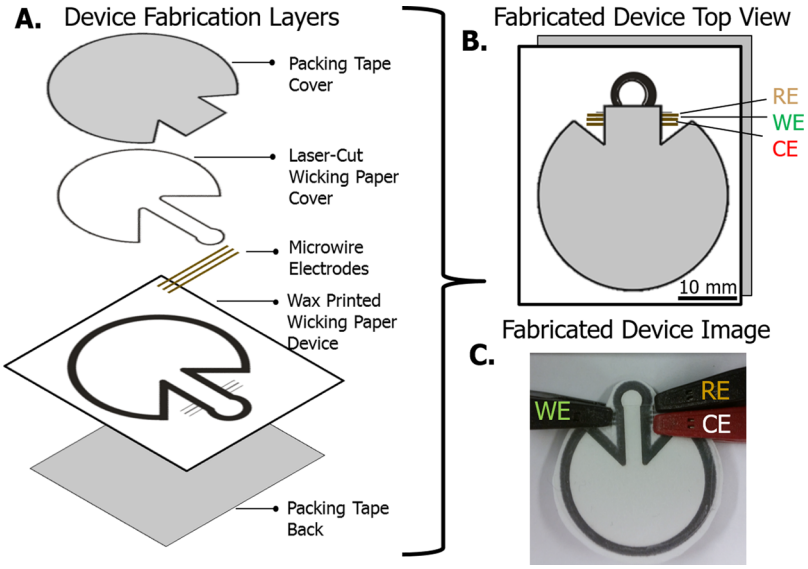

electronics can also be miniaturized and battery powered for portable and simple detection of multiple analytes (i.e., a hand-held glucose meter).[13] Although many ePADs have been developed to perform detection in quiescent solution, few have been developed for detection in flow. Flow in paper devices is driven by capillary force,[14] gravity,[15] and/or pressure differences from an inlet and outlet.[16] While these systems have been used effectively, ePADs developed for flow injection analysis (FIA) are less common.[17] FIA has the advantage of being able to detect multiple sample additions with time, for example, Dossi et al. presented a system for FIA detection at pencil drawn electrodes in a paper-based channel.[17] Solution was pulled through the channel by an attached wicking pad, and this system showed good repeatability and reproducibility for up to seven measurements. However, to the best of our knowledge, no other ePADs have demonstrated the steady-state flow in combination with FIA detection.

Several methods for electrode fabrication and incorporation into ePAD devices have been developed.[18,19] The most common method involves using a screen[11] or stencil[20] to pattern conductive carbon or metallic inks onto paper. Carbon has been the most common ePAD electrode material, due to its low-cost, widespread availability, and wide potential window for detection.[18] Metallic electrodes, however, have also been used and provide their own unique advantages including: higher conductivity, alternative catalytic activity, and subsequent electrochemistry from carbon. Metal electrodes, most commonly gold and silver, have been deposited onto the surface of paper using thin film deposition techniques,[21] nanoparticle growth,[22,23] or inkjet printing.[24] Similar to previous work presented by our group in which microwires were incorporated into polymer microfluidic devices,[25] microwires have also been incorporated into paper-based devices. Crooks and co-workers first published the use of microwire electrodes within paper devices.[26] These prefabricated electrodes could be easily cleaned and modified prior to incorporation into an ePAD and without damaging the paper substrate. Previous work by our group further studied the use of microwires in contact with paper and found that they provided higher flux of species to the electrode surface and improved electrochemical performance from paper-based electrodes reported in the literature and fabricated carbon ink electrodes.[27,28] Although microwire electrodes have been incorporated into ePAD devices,[26,28] these devices employed quiescent solutions.

Herein, we report the first use of microwire electrodes in a paper-based flow-through device. The device integrates a unique geometry adapted from a previously reported device concept by Mendez et al.[29] Originally proposed as a method to create a steady solution flow for lateral flow assays, the developed device makes use of a regularly increasing capillary network in the shape of a 270° fan connected to an inlet channel. This fan geometry is used to compensate for the decay in flow rate within the analysis channel that coincides with the distance a fluid front travels through a capillary network (Lucas-Washburn Law).[30−32] However, to the best of our knowledge, this device design has never been implemented with any analyte detection motif aside from dye-based flow characterization. The fan design generates a steady flow of solution through an inlet channel, and the integration of electrodes within this channel offers the possibility to detect multiple samples with time and without a decay in fluid transport that would also result in a decay in mass transport to the electrode and in measured current. Additionally, the use of a sandwiched paper format on both sides of the microwire electrodes allows for full immersion of the electrode in a flow through ePAD, increasing the available electrode working area. As proof of concept, an enzyme kinetics study was conducted with the device to determine time-based reaction variables using β-galactosidase and *p*-aminophenyl-galactopyranoside (PAPG) as enzyme and substrate, respectively. This reaction generates *p*-aminophenol (PAP) which is a common product in electrochemical immunoassays as well as a health indicator or contaminant in clinical and environmental samples, respectively, due to its use or byproduct production in pesticides, dyes, and pharmaceuticals.[33] As such, PAP serves as a model analyte for broader applications.

DOI: 10.1021/acs.analchem.6b03010
Anal. Chem. 2016, 88, 10639−10647

EXPERIMENTAL SECTION

Materials. Potassium chloride (KCl), potassium nitrate (KNO_3), potassium hydroxide (KOH), iron(III) chloride hexahydrate ($FeCl_3 \cdot 6H_2O$), potassium ferricyanide ($K_3Fe(CN)_6$), 30% hydrogen peroxide (H_2O_2), and Whatman #1 filter paper were purchased from Fisher Scientific (Fairlawn, NJ). Benzoquinone (BQ) and *p*-aminophenol (PAP) were purchased from Alfa Aesar (Ward Hill, MA) and EMD Millipore (Billerica, MA), respectively. Hydroquinone (HQ), *β*-galactosidase enzyme, and *p*-aminophenyl-galactopyranoside (PAPG) substrate were purchased from Sigma-Aldrich. Both enzyme, substrate, and stock solution aliquots were stored at −20 °C prior to use. Fresh aliquots were thawed prior to use daily. Potassium ferrocyanide ($K_4Fe(CN)_6$) was purchased from Mallinckrodt Chemical Works (St. Louis, MO). High-purity silver ink was purchased from SPI Supplies (West Chester, PA). Electrode materials, 99.99% pure gold (25 μm), and platinum (30 μm) microwires (diameter) were purchased from California Fine Wire Company (Grover Beach, CA). All reagents were used as received without further purification. All electrochemical measurements were done using either an eDAQ EA161 Potentiostat and EC201 e-Corder (Denistone East, Australia) or a CHI 660B Electrochemical Workstation (Austin, TX). 2-in.-wide Scotch brand heavy duty clear shipping packaging tape was purchased from 3 M (St. Paul, MN). Devices were printed using a Xerox (Norwalk, CT) ColorCube 8870 wax printer and stencils, and paper and tape components were cut using a 30 W Epilog (Golden, CO) Zing Laser Cutter and Engraver.

Microwire ePAD Fabrication. Similar to previously described work, ePADs were designed using CorelDRAW (Corel, Ottawa, Ontario), a graphic design program, and fabricated on Whatman #1 filter paper.[28] Fluid flow and containment were achieved by printing hydrophobic wax barriers using a wax printer. Wax printed designs of 4-pt line thickness were melted through the filter paper on a 150 °C hot plate for 90 s to create wax barriers. Packing tape was used to seal the bottom of the device and prevent leaking. On the printed side, microwires were spaced 1 mm apart across the channel device using printed alignment marks as guides and either taped in place with a packing tape cover or covered with a laser-cut Whatman wicking layer, followed by the laser-cut packing tape cover (Scheme 1A,B). The paper-based sample inlet used a 6 mm diameter (4.1 mm inner diameter after melting) wax printed well connected to a channel that is 11 mm long by 5 mm wide (11.2 mm length by 3.1 mm inner width after melting). The channel flows into the center of a 30 mm diameter circle (27.8 mm inner diameter after melting) with a 90° section removed to form a 270° wicking fan from the channel end. The laser-cut wicking top of the device has the same dimensions as the paper region bound by the melted wax described in parentheses above. The laser-cut packing tape cover consists of a rectangle (9 mm × 7 mm) connected 8 mm into a 34 mm diameter circle. The packing tape cover is made so that the tape covers approximately 1 mm past the wax printed and melted outer edge of the device to create a protective seal and hold the microwire electrodes and wicking layer in place on top of the wax printed layer of the device. The sample well inlet is left uncovered for sample addition. Silver paint was applied to wire ends to create touchpads that could be connected to the potentiostat (Scheme 1C).

Characterization of Device with Flow. Visual determination and color analysis software were used to characterize flow within single and double-paper layer devices. The Lucas-Washburn flow behavior within straight channels with single and double layers of paper were characterized visually by dipping the sample inlet into a dye solution and measuring the height of the fluid front with time. The channels were fabricated with the same sample inlet and channel width dimensions as the quasi-steady flow device described above, but with a channel length extended to 90 cm (Figure S1). Steady flow behavior was measured within the ePAD device made with either a single layer of paper or double layer by measuring the increase in colored area with time from photos using ImageJ analysis software. ImageJ was used to isolate the red region formed within the device and measure the normalized growth in area until the device was completely red within the wax defined region.

Device flow was also characterized using amperometry by the repeated addition of 5 or 10 μL of a blank injection consisting of 0.5 M KCl or a sample containing 5 mM $K_4Fe(CN)_6$/$K_3Fe(CN)_6$ in 0.5 M KCl to the sample inlet. Electrochemical detection was determined using Au or Pt microwire electrodes. The average current was measured from the steady-state flow and resulting steady-state current produced. Linear-sweep voltammetry (LSV) was taken of 5 mM $K_4Fe(CN)_6$/$K_3Fe(CN)_6$ in 0.5 M KCl at Au microwire electrodes, in a saturated paper-based channel or while solution was flowing within the ePAD device. The saturated channel containing electrodes was made by removing the fan shaped region at the end of the channel and adding solution (∼20 μL) to the inlet until no more solution was removed from the inlet to wick down the channel.

Flow ePAD Calibration. Calibration detection of flow devices was carried out using amperometry with droplet addition as described above for repeatability experiments. Five or 10 μL droplets of solution were added to the device, and the average plateau current was plotted against concentration, for both Pt and Au working electrodes and with either $K_4Fe(CN)_6$/$K_3Fe(CN)_6$ or HQ/BQ in 0.5 M KCl or PAP in pH 7.4 laboratory-prepared phosphate buffered saline (PBS, 8.00 g of NaCl, 0.24 g of KCl, 1.44 g of Na_2HPO_4, and 0.24 g of KH_2PO_4, per liter of distilled water). Plateau currents were then normalized to a standard added at the end of each use and plotted against concentration to create a normalized calibration curve. Standards were 5 mM $K_4Fe(CN)_6$/$K_3Fe(CN)_6$ and HQ/BQ for the same species calibration curves and 1 mM $K_4Fe(CN)_6$/$K_3Fe(CN)_6$ in 0.5 M KCl for PAP calibration.

Enzyme Kinetics Detection. The ePADs were used to perform a kinetic study on *β*-galactosidase activity using *p*-aminophenyl-galactopyranoside (PAPG) as the substrate. The product of this enzymatic reaction, *p*-aminophenol (PAP), is a redox active molecule. The flow device design contained one Pt microwire reference electrode and two Pt microwires working and two Pt microwire counter electrodes. Cyclic voltammograms (CVs) of 1 mM PAPG or 1 mM PAP in pH 7.4 PBS were acquired at 0.1 V/s from 0.2 to 0.7 V vs Pt and from −0.1 to 0.4 V vs Pt, respectively, to study electrochemical properties of both species. The optimal applied overpotential for PAP detection from the PAPG background current was determined by detecting the plateau current with droplet flow through the device using amperometry at 0.1, 0.2, 0.3, and 0.4 V vs Pt. A 0.3 V optimal applied overpotential was determined and employed for the duration of amperometric measurements for PAP

DOI: 10.1021/acs.analchem.6b03010
Anal. Chem. 2016, 88, 10639−10647

detection. A PAP calibration curve was established by measuring 0−1 mM PAP solutions in pH 7.4 PBS. To ensure reproducibility of enzymatic detection within the devices, three separate 100 μL solutions containing 1 mM PAPG and 5 U/mL β-galactosidase were prepared in fresh pH 7.40 PBS before analysis and were added in 5 μL aliquots to separate devices every 60−100 s until the measured current reached a plateau. Similarly, to obtain the rate of reaction at different concentrations of substrate, equal volumes of 10 U/mL β-galactosidase solution and 0.2−10 mM PAPG solutions were mixed (end concentration of 5 U/mL and 0.1−5 mM PAPG), and the current was measured during the initial linear enzymatic response. At least five time points were collected for each substrate concentration to calculate the rate of reaction from the linear slope obtained from change in current with time. Current was converted to PAP concentration using the previously obtained PAP calibration curve. Measurements were done in three separate devices, and the measured rates for each device were averaged. A Lineweaver−Burk plot (i.e., 1/[substrate] vs 1/rate plot) was established and the Michaelis−Menten constant (K_m) was extracted from the plot.[34]

RESULTS AND DISCUSSION

Device Design Theory. Aside from the low-cost, a key advantage to using paper as an analytical platform lies in exploiting the capillary force generated from the hydrophilic network of cellulose fibers to imbibe solution into the device. Both lateral flow assays and many paper-based devices take advantage of this passive flow to implement sample mixing, reaction timing, and washing steps that would otherwise necessitate the use of external pumps and pipetting steps.[4] However, a disadvantage to using paper is that flow velocity decreases with time within capillaries of constant cross-sectional area (such as in lateral flow assays and paper-based channels). When considering sensor response, this decay can increase the assay time as well as change detection response as a function of time. While the capillary driving force itself remains constant within a channel of constant cross sectional area, there is an increase in viscous drag force due to the increase in wetted area and the distance the fluid front moves from the inlet reservoir. This behavior is described by the Lucas-Washburn equation:[31]

$$l(t) = \sqrt{\left(\frac{\gamma r \cos\theta}{2\mu}\right)t} \quad (1)$$

where the distance the fluid front travels with time ($l(t)$) is directly proportional to the square root of time (t), cosine of the solution contact angle with paper (θ), solution surface tension (γ), and the mean capillary pore radius or effective pore radius of the paper (r), as well as indirectly proportional to the square root of the viscosity (μ).[31] Figure 1A shows the experimentally measured increase in fluid front distance within a straight channel for both one- and two-layer devices (device images shown in Figure S1). As previously observed by Camplisson et al., a noticeable increase in flow rate is achieved when using two layers of paper to imbibe solution within a channel.[35] This increase was attributed to an increase in the effective pore radius, due to the gap between the sheets acting as a larger capillary. They experimentally determined an increase from 0.11 μm (average horizontal pore radius within Whatman # 1 filter paper) for imbibition in a single layer of paper to 0.34 μm, due to the inclusion of the gap between the two layers of paper.

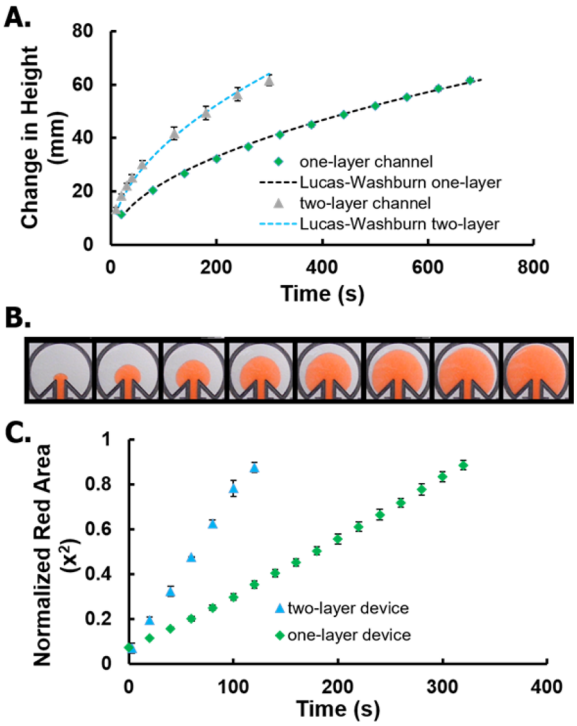

Figure 1. Flow rate characterization for (A) straight channels and (B and C) quasi-steady flow devices with either one- or two-layers of paper. (A) Straight channel flow behavior is determined experimentally and modeled using (eq 1). (B) Quasi-stationary flow device images were taken every 20 s, and (C) flow rate was calculated from these images via change in red area within the device and normalized to the total device area. Time 0 s = time the solution reaches the end of the channel for start of the steady flow regime (n = 4 devices/measurement).

While the prior work determined the average pore radius with evaporative variables, the device design employed in this work uses tape to seal the device, thus minimizing evaporation. Using eq 1 to fit the experimental data with solution terms for water at room temperature (γ = 0.0728 N·s, μ = 0.001 N·s/m^2) and θ = 0 for Whatman #1 filter paper, the effective pore radius was calculated to be 0.15 ± 0.01 and 0.38 ± 0.06 μm for one- and two-layer devices, respectively. The slightly larger effective pore radius is probably due to the addition of tape acting as another capillary wall, where it is not adhered to the fibers and serves to keep solution and humidity within the device. The calculated gap height between the paper layers, using a weighted average of the calculated effective pore radius values (Equation S1),[35] was determined to be 12 μm, which is reasonable given the visual spacing shown in cross sections as discussed below and matches the reported value obtained by Camplisson et al.[35]

One way to overcome the increase in viscous drag force and therefore decay in flow rate was proposed by Mendez et al.[29] This relies on a steady increase in the fluid front area in the shape of a 270° fan attached to the channel exit, providing a counterbalance to the capillary pressure. The flow behavior for the fully wetted capillary network within the channel can be described by Darcy's Law:[36]

DOI: 10.1021/acs.analchem.6b03010
Anal. Chem. 2016, 88, 10639−10647

$$Q = \frac{\kappa w h P_c}{\mu L} \quad (2)$$

where the volumetric flow rate (Q) is directly proportional to the capillary pressure ($P_c = 2\gamma \cos\theta/r$), interstitial permeability (κ, approximated to be $r^2/8$), channel width (w = 3.1 mm), and height (h = 150 μm or [2(150 μm) + 12 μm] for one- and two-paper layers respectively), while indirectly proportional to the channel length (L = 11.2 μm) and the solution viscosity. The fabrication scheme for a quasi-steady flow device that was characterized for flow rate based on the change in fluid area within the device with time is shown in Scheme 1. Similarly, Figure 1B,C show photographs of the wetting and the normalized wetting area as a function of time. A steady increase in area with time is observed for both one- and two-layer devices. Assuming that a given change in area corresponds to a set volume of solution flowing through the channel (i.e., assuming constant h throughout the device), a linear increase in area within the wicking fan corresponds to a steady flow of solution through the channel. The use of two layers of paper increased the flow rate by 273% compared to a single layer device. As discussed previously, the increase in flow rate for the two-layer relative to the one-layer device is due to the gap present between paper layers and therefore larger capillary height. Although initial flow through the channel is not steady, once the fluid front reaches the fan region, a steady flow rate is maintained. This was therefore used as a starting point for carrying out analytical measurements.

To the best of our knowledge, this is the first time change in fluid area within a paper-based device has been used to characterize flow rate through a sample inlet. Previous work has measured the rate a dye fluid front moves through a prewetted channel.[37] However, this method can only monitor the dye speed through the length of the channel and cannot measure flow rate once the dye reaches the wicking pad. Another method made use of alternating the sample inlet between solutions with or without dye to form bands of dye.[29] The flow rate was then determined on the basis of the speed the bands moved through the channel with time. While this method worked well for a slow flow rate material such as nitrocellulose, the method required precise changing of solutions to form the bands, which do not have time to form within the inlet channel in faster flow rate materials such as the Whatman grade 1 filter paper used in this study. An alternative study measured the change in radius and, therefore, change in volume of imbibed solution within a hemispherical-glass matrix from a point source.[38] The study also determined that radial change in volume was constant with time, matching well with our results for a thin membrane change in area. Our presented method, therefore, serves as a more universal and simple means for monitoring flow rate through a sample inlet within paper devices, especially in device geometries that deviate from Lucas-Washburn behavior.

Microwire ePAD Electrochemical Behavior with Flow. Electrochemical detection in ePADs is usually carried out in quiescent solution, and as such, detection under steady flow conditions has not been studied extensively in paper. A comparison to electrochemical detection at Au microwire electrodes with and without flow in ePADs was carried out using LSV in 5 mM $K_4Fe(CN)_6/K_3Fe(CN)_6$ in 0.5 M KCl. Figure 2A shows distinctive voltammograms indicative of mass-transport and diffusion limited currents with flow and quiescent solution conditions, respectively. Unlike the peak-current

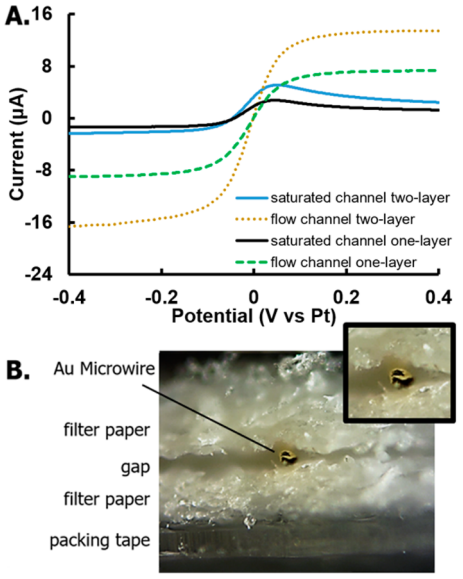

Figure 2. Electrochemical detection showing (A) the LSV current profiles for one- and two-layer devices either with quasi-steady flow or without flow in a saturated channel using 5 mM $K_4Fe(CN)_6/K_3Fe(CN)_6$ in 0.5 M KCl, detected at 25 μm diameter Au microwire electrodes (Pt counter and reference). (B) Image of channel cross-section, cut down the center, showing a 25 μm Au electrode sandwiched between two paper layers with an enlarged inset of the cut, circular end of the Au microwire electrode in the upper right corner.

behavior obtained for the quiescent solution, a sigmoidal steady-state current is obtained within the flow device due to added convection of analyte to the electrode surface. The measured LSVs showed a peak current increase from 3.77 ± 0.58 for one-layer devices in the absence of flow to 12.17 ± 0.71 μA with the addition of flow. For two-layer devices, peak current increased from 5.92 ± 0.81 to 20.66 ± 0.32 μA with the addition of flow. The slightly larger increase in peak current with flow addition for a two-layer device (249% increase) when compared with a one-layer device (222% increase) is probably due to a further swelling of the gap between the layers of paper with flow that cannot occur in a one-layer device, as the electrode is held more tightly in place with packing tape. The slightly larger increase in peak current from one- to two-layers with (69.7% increase) and without flow (56.9% increase) is also indicative of the increase in gap-height that acts like a larger capillary with flow. The optimal device design incorporated sandwiching of the electrodes between two layers of paper (Figure 2B) in order to maximize the electrode surface area and flow rate of species to the electrode surface.

Figure 3A shows the amperometric current response of the device with no flow and the subsequent spike and plateau of current from the flow of solution across the electrodes, due to droplet addition to the well inlet. Addition of the droplet to the device creates an increase in current due to an increase in mass-transport. Because of the perturbation of the double layer with flow, a small spike can be seen at the start of flow, immediately after droplet addition. The spike decays while the flow rate stabilizes, reaching a plateau current. During the plateau, steady-flow behavior is maintained and an average current measurement is recorded. This plateau current is dependent on both the flow rate and the amount of faradaic and nonfaradaic current being passed (Figure 3B). The plateau is followed by a decay of signal back to the baseline when flow stops due to

DOI: 10.1021/acs.analchem.6b03010
Anal. Chem. 2016, 88, 10639−10647

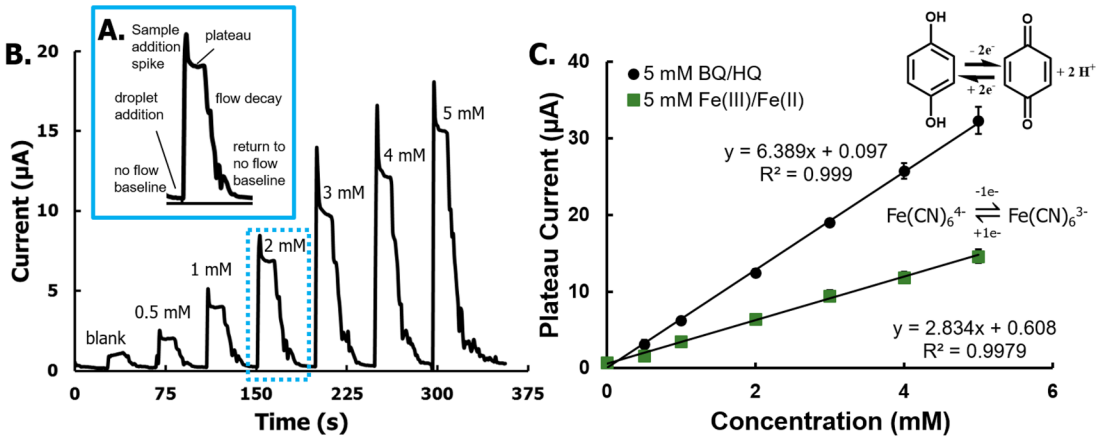

Figure 3. Quasi-stationary flow ePAD amperometric detection showing (A) the detailed flow-current profile blown up from the 2 mM injection of (B) the full calibration amperometric profile for increasing concentrations of $K_4Fe(CN)_6/K_3Fe(CN)_6$ in 0.5 M KCl and (C) plotted as the average peak plateau current in the calibration plots for increasing concentrations of $K_4Fe(CN)_6/K_3Fe(CN)_6$ (n = 9 devices) or HQ and BQ (n = 4 devices) in 0.5 M KCl detected at 25 μm diameter gold microwire electrodes at −600 mV.

liquid depletion at the inlet. While the initial increase in current is rapid as the droplet fills the already wet capillary network and flows through, the decay follows a more gradual decrease. Microscopy of flow through paper shows that this more gradual decrease is due to the capillary force at the fluid front having to break the surface tension of filled pores in the paper to remove solution.

The device repeatability under steady-flow was determined through repeated injections of a blank (0.5 M KCl) or a sample (5 mM $K_4Fe(CN)_6/K_3Fe(CN)_6$ in 0.5 M KCl). An example amperogram is shown in Figure S2. The plateau current without faradaic reactions occurring created a small change in cathodic background current (no flow) of −4.9 ± 0.5 nA (n = 11) when blank 5 μL injections were added (Figure S3B). The average combined cathodic faradaic and nonfaradaic current was measured to be −6.66 ± 0.22 μA (n = 16 injections) at the plateau from the sample flow across the electrode with repeated 5 μL injections. However, an interesting phenomenon occurred when doing anodic detection (Figure S3A). A smaller overall current response was measured from both blank (1.69 ± 0.27 nA (n = 11)) and sample (−1.97 ± 0.14 μA (n = 10)) injections. This behavior was seen for both Au and Pt working electrodes and for different species detected ($K_4Fe(CN)_6$ and HQ). While the cause of this phenomenon is unclear, the device still behaved consistently with repeated injections for oxidation. This could possibly be due to some interaction of the electrode with the cellulose matrix. Cellulose is a polysaccharide comprised of glucose, which has been found to adsorb to both gold and platinum surfaces from near neutral (pH 7.4) to more basic solutions.[39,40] This phenomenon could explain the initial decline in current, due to a decrease in active sites for electrochemical detection that then stabilizes after an adsorption layer is formed.

Microwire ePAD Calibration. Next, the ePAD was used for the detection of $K_4Fe(CN)_6/K_3Fe(CN)_6$ and HQ/BQ as model inner sphere inorganic and organic redox species respectively. Figure 3C shows the resulting calibration plots from several devices (n = 13) with good linearity and correlation ($R^2 \geq 0.998$). The slopes also correlate with increasing electron-transfer processes, where the slope approximately doubles when going from $K_4Fe(CN)_6/K_3Fe(CN)_6$ (slope = 2.834 μA/μM, 1 electron process) to HQ/BQ (slope = 6.389 μA/μM, 2 electron process). While good reproducibility was found within flow devices, average measurements between devices, however, could produce RSDs that were greater than desired, as seen in Figure S4A, where average RSDs were 10.65%. As each sensor is assembled by hand and sometimes by different individuals, this was attributed to small differences in fabrication, such as the amount of pressure used to seal the device or variations in alignment. One way to account for device-to-device variations is to normalize the signal using a standard solution addition (Figure S4B), which reduced average RSDs to 4.56%. Calibration plots for both oxidation and reduction of $K_4Fe(CN)_6/K_3Fe(CN)_6$ at both Au and Pt electrodes still show good linearity ($R^2 \geq 0.998$) with average RSD of 7.46% (Figure S5). It is of interest to note that all of the slopes are nearly equivalent with oxidation and reduction slope values of 0.1983 and 0.2031 mM^{-1} at Au and 0.2001 and 0.1983 mM^{-1} at Pt microwire electrodes respectively when each device is normalized to the same 5 mM standard injection. The same slopes are also nearly equivalent to each other when more than one wire is used to form the working electrode (Figure S6). Figure S6B shows the effect doubling the electrode area has on the measured slope, 1.88 for one-wire to 2.95 μA/mM for a two-wire working electrode device. These differences in electrode area were normalized when using a standard; however, both one-wire (normalized slope = 0.1998 mM^{-1}) and two-wire (normalized slope = 0.1871 mM^{-1}) working electrodes produced similar normalized slopes (Figure S6C). The two-wire slope in Figure S6C is probably slightly lower than one-wire due to an increase in background current determined when using a working potential > ±0.5 V vs Au or Pt pseudoreference electrodes for both Au and Pt working electrodes, respectively (Figure S7). Lower applied potentials resulted in lower background signal, and the use of two working electrodes resulted in greater current that could be more easily measured by the potentiostat.

Enzymatic Detection. As proof of concept, the quasi-steady flow device was implemented for the continuous monitoring of enzymatic activity. Enzymatic assays have been widely used as analytical detection methods due to their selectivity and sensitivity to target analytes. Examples of these assays include: clinical assays where enzymes react with target health indicators to produce a detectable product,[41] as

DOI: 10.1021/acs.analchem.6b03010
Anal. Chem. 2016, 88, 10639−10647

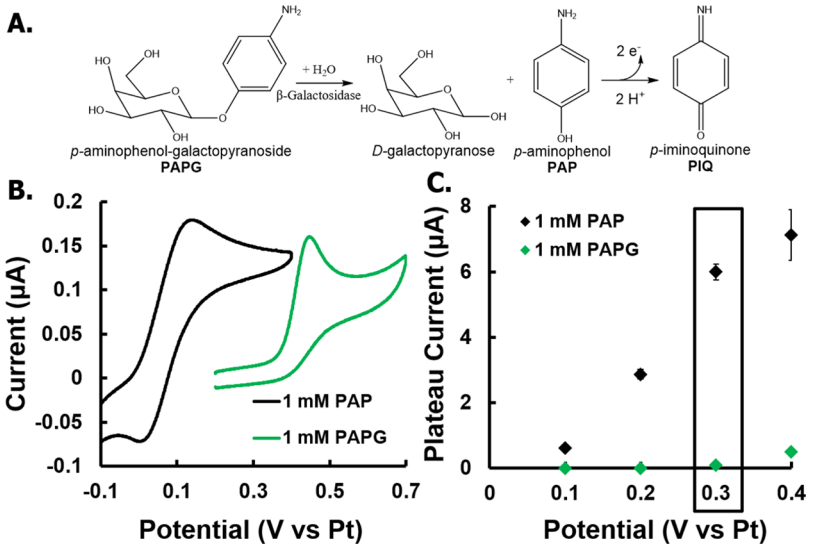

Figure 4. Optimal potential determination of PAP formed from (A) the reaction of PAPG with β-galactosidase and detected electrochemically through a $2e^-$ oxidation reaction. (B) Cyclic voltammograms of 1 mM PAP or PAPG in pH 7.4 PBS buffer were measured using Pt microwire electrodes in saturated paper-based channel devices without flow and (C) the resulting hydrodynamic voltammograms using amperometric detection with flow (n = 4). The optimal potential for amperometric detection is designated at 0.3 V.

detectable tags in enzyme-linked immunosorbent assays (ELISAs),[42] as an indicator of gene expression via the production or deletion of specific genes for enzyme production,[43] and in bacterial assays where the presence of bacterially produced enzymes is used to identify bacterial species.[44] β-Galactosidase is commonly used as a tag in ELISAs, a reporter marker in gene expression, and as a bacterial indicator for total coliform counts and *E. coli* species identification.[45] β-Galactosidase hydrolyzes the β-glycosidic bond between a galactose and its organic moiety, and its enzyme activity is then measured via product formation. The steady-flow device was used to measure the activity of β-galactosidase via the production of *p*-aminophenol (PAP) from the substrate *p*-aminophenyl-galactopyranoside (PAPG) (Figure 4A). PAP is electrochemically active and thus detectable through a two electron oxidation reaction. Its use for the electrochemical detection of enzymatic activity has been previously well described.[46] As shown in Figure 4B, both the substrate PAPG and product PAP are electrochemically active with peak potentials at 0.45 and 0.15 V vs Pt, respectively, and an optimal amperometric overpotential was determined to be 0.3 V vs Pt (Figure 4C). PAP calibration was then determined using flow devices with dual microwire Pt working electrodes at 0.3 V (Figure S8), and a 31 μM limit of detection was calculated (mean + 3SD).

The enzyme kinetics of β-galactosidase for the electrochemical reaction were studied amperometrically at 0.3 V vs Pt by continuously adding the reaction solution (varying PAPG concentration with 10 U/mL enzyme in PBS) to the device and monitoring the changes in plateau current with time. Once the measured current was converted to PAP concentration using a calibration curve, the reaction rate could be obtained and plotted against the starting substrate concentration (Figure 5A). Figure 5A is a Michaelis–Menten plot showing the rate of reaction beginning to plateau above 1 mM PAPG, indicating a saturation in the catalytic capability of the enzyme in solution.[47]

The Lineweaver–Burk plot in Figure 5B serves as a useful graphical representation, whereby the maximum rate of reaction (V_{max}) and Michaelis–Menten constant (K_m) can be easily

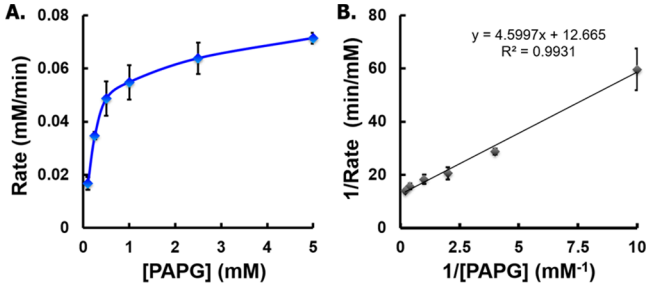

Figure 5. Enzyme kinetics plots determined by measuring β-galactosidase reaction with PAPG to form PAP in (A) Michaelis–Menten and (B) Lineweaver–Burk plots (n = 4).

calculated from the y-intercept ($1/V_{max}$) and slope (K_m/V_{max}) or x-intercept ($-1/K_m$), from experimentally determined changes in rate (V) measured from using different concentrations of substrate ($[S]$).[34] The V_{max} and K_m values were experimentally determined to be 0.079 mM/min and 0.36 mM, respectively. An enzyme turnover number (k_{cat}), which is the maximum number of substrate molecules turned over by an enzyme molecule per second, was calculated from the determined V_{max} to be 94 s^{-1}. A separate study in quiescent solution by Laczka et al., using a Au microelectrode array as the working electrode for the electrochemical detection of PAP, found a similar K_m value of 0.43 mM, which indicates a similar substrate affinity when reacting PAPG with β-galactosidase.[48] For the same reaction, Viratelle and Yon also found similar K_m (0.33 mM) and k_{cat} (90 s^{-1}) values using a spectrophotometer at 306 nm for PAP detection.[49] The similarities of our calculated values to literature, for more complex or expensive detection platforms, indicate that the proposed disposable and simple to fabricate device provides a viable and alternative analytical method for detecting enzyme kinetics in real time.

It is also plausible to utilize the quasy-steady flow device to perform immunoassays including ELISAs by depositing biorecognition elements capable of generating electrochemical signals upon binding to target analyte on the surface of the working electrode. This device could use target binding

DOI: 10.1021/acs.analchem.6b03010
Anal. Chem. 2016, 88, 10639–10647

antibodies, for example, attached to the microwire working electrode or the paper itself. Similar to a lateral flow assay (LFA), reagents can be stored within the device, and upon addition of sample, analyte can be reacted, captured, and washed of unbound material prior to electrochemical product formation detection at the microwire electrodes. Detection of a dengue biomarker in a lateral flow assay has been previously demonstrated by Sinawang et al. using an antibody-conjugated screen-printed gold electrode at which the analyte was captured and later sandwiched with a secondary antibody labeled with ferrocene.[50] Platinum electrodes have also been employed to carry out ELISA in a flow-based system for detecting cortisol.[51] In electrochemical ELISAs, enzymes are often conjugated to a secondary antibody to convert the substrate into a redox active species product.[51−53]

CONCLUSIONS

The use of a steadily increasing capillary network, to generate quasi-steady flow, has been studied for the first time in ePADs. The device is simple and inexpensive to fabricate and has been employed for electrochemical detection at microwire electrodes. The use of single- and double-paper layers can be used to control flow rate by changing the effective pore radius of the device. The resulting increase in fluid transfer through the device when two-layers of paper are used is achieved by incorporating the gap between the layers of paper that acts as a larger capillary. Both colorimetric and electrochemical detection within the device, using image processing software and microwire electrodes, respectively, provided reproducible results and can be used in future device development to monitor flow response within paper-based devices. Additionally, calibration plots normalized to a standard provided improved measurement reproducibility between devices. Future device design could incorporate a separate layer with stored standard reagents that could be measured at the end of the device use for normalization purposes. As proof-of-concept, the devices were used to measure enzyme activity for β-galactosidase and PAP, which provided kinetic values similar to those found in the literature, demonstrating the usefulness of this device. Moreover, this device design could incorporate modified microwire electrodes to improve detection sensitivity or to capture species from solution at the electrode surface while utilizing device flow. This ePAD, therefore, serves as an alternative detection platform to current colorimetric methods and as a faster analysis approach for measuring a set volume of solution in laboratory tests such as lateral flow assays.

ASSOCIATED CONTENT

Supporting Information

The Supporting Information is available free of charge on the ACS Publications website at DOI: 10.1021/acs.analchem.6b03010.

Details of device flow characterization, pore radius determination, electrochemical measurements, repetitive signal response, and calibration (PDF)

AUTHOR INFORMATION

Corresponding Author

*E-mail: Chuck.Henry@colostate.edu. Phone: +1-970-491-2852.

Notes

The authors declare no competing financial interest.

ACKNOWLEDGMENTS

This work was partially supported by the National Institutes of Health (ES023496). Additional support was received from Colorado State University. The authors also thank Robert Channon for editorial assistance.

REFERENCES

(1) Rackus, D. G.; Shamsi, M. H.; Wheeler, A. R. *Chem. Soc. Rev.* **2015**, *44*, 5320−5340.
(2) Volpatti, L. R.; Yetisen, A. K. *Trends Biotechnol.* **2014**, *32*, 347−350.
(3) Martinez, A. W.; Phillips, S. T.; Butte, M. J.; Whitesides, G. M. *Angew. Chem., Int. Ed.* **2007**, *46*, 1318−1320.
(4) Cate, D. M.; Adkins, J. A.; Mettakoonpitak, J.; Henry, C. S. *Anal. Chem.* **2015**, *87*, 19−41.
(5) Nery, E. W.; Kubota, L. T. *Anal. Bioanal. Chem.* **2013**, *405*, 7573−7595.
(6) Yetisen, A. K.; Akram, M. S.; Lowe, C. R. *Lab Chip* **2013**, *13*, 2210.
(7) Fridley, G. E.; Le, H. Q.; Fu, E.; Yager, P. *Lab Chip* **2012**, *12*, 4321−4327.
(8) Carrilho, E.; Martinez, A. W.; Whitesides, G. M. *Anal. Chem.* **2009**, *81*, 7091−7095.
(9) Meredith, N. A.; Quinn, C.; Cate, D. M.; Reilly, T. H.; Volckens, J.; Henry, C. S. *Analyst* **2016**, *141*, 1874−1887.
(10) Lisowski, P.; Zarzycki, P. K. *Chromatographia* **2013**, *76*, 1201−1214.
(11) Dungchai, W.; Chailapakul, O.; Henry, C. S. *Anal. Chem.* **2009**, *81*, 5821−5826.
(12) Rattanarat, P.; Dungchai, W.; Cate, D.; Volckens, J.; Chailapakul, O.; Henry, C. S. *Anal. Chem.* **2014**, *86*, 3555−3562.
(13) Nie, Z.; Deiss, F.; Liu, X.; Akbulut, O.; Whitesides, G. M. *Lab Chip* **2010**, *10*, 3163−3169.
(14) Carvalhal, R. F.; Simão Kfouri, M.; de Oliveira Piazetta, M. H.; Gobbi, A. L.; Kubota, L. T. *Anal. Chem.* **2010**, *82*, 1162−1165.
(15) Lankelma, J.; Nie, Z.; Carrilho, E.; Whitesides, G. M. *Anal. Chem.* **2012**, *84*, 4147−4152.
(16) Renault, C.; Anderson, M. J.; Crooks, R. M. *J. Am. Chem. Soc.* **2014**, *136*, 4616−4623.
(17) Dossi, N.; Toniolo, R.; Pizzariello, A.; Impellizzieri, F.; Piccin, E.; Bontempelli, G. *Electrophoresis* **2013**, *34*, 2085−2091.
(18) Adkins, J.; Boehle, K.; Henry, C. *Electrophoresis* **2015**, *36*, 1811−1824.
(19) Mettakoonpitak, J.; Boehle, K.; Nantaphol, S.; Teengam, P.; Adkins, J. A.; Srisa-Art, M.; Henry, C. S. *Electroanalysis* **2016**, *28*, 1420.
(20) Nie, Z.; Nijhuis, C. A.; Gong, J.; Chen, X.; Kumachev, A.; Martinez, A. W.; Narovlyansky, M.; Whitesides, G. M. *Lab Chip* **2010**, *10*, 477−483.
(21) Siegel, A. C.; Phillips, S. T.; Dickey, M. D.; Lu, N.; Suo, Z.; Whitesides, G. M. *Adv. Funct. Mater.* **2010**, *20*, 28−35.
(22) Cunningham, J. C.; Brenes, N. J.; Crooks, R. M. *Anal. Chem.* **2014**, *86*, 6166−6170.
(23) Ge, L.; Wang, S.; Yu, J.; Li, N.; Ge, S.; Yan, M. *Adv. Funct. Mater.* **2013**, *23*, 3115−3123.
(24) Hu, C.; Bai, X.; Wang, Y.; Jin, W.; Zhang, X.; Hu, S. *Anal. Chem.* **2012**, *84*, 3745−3750.
(25) García, C. D.; Henry, C. S. *Anal. Chem.* **2003**, *75*, 4778−4783.
(26) Fosdick, S. E.; Anderson, M. J.; Renault, C.; DeGregory, P. R.; Loussaert, J. A.; Crooks, R. M. *Anal. Chem.* **2014**, *86*, 3659−3666.
(27) Adkins, J. A.; Henry, C. S. In *International Conference on Miniaturized Systems for Chemistry and Life Sciences*; RSC Publishing: San Antonio, TX, 2014; pp 1583−1585.
(28) Adkins, J. A.; Henry, C. S. *Anal. Chim. Acta* **2015**, *891*, 247−254.
(29) Mendez, S.; Fenton, E. M.; Gallegos, G. R.; Petsev, D. N.; Sibbett, S. S.; Stone, H. A.; Zhang, Y.; López, G. P. *Langmuir* **2010**, *26*, 1380−1385.

DOI: 10.1021/acs.analchem.6b03010
Anal. Chem. 2016, 88, 10639−10647

(30) Li, K.; Zhang, D.; Bian, H.; Meng, C.; Yang, Y. *Sci. Rep.* **2015**, *5*, 14085.
(31) Washburn, E. W. *Phys. Rev.* **1921**, *17*, 273−283.
(32) Lucas, R. *Colloid Polym. Sci.* **1918**, *23*, 15−22.
(33) Lin, T.; Li, Z.; Song, Z.; Chen, H.; Guo, L.; Fu, F.; Wu, Z. *Talanta* **2016**, *148*, 62−68.
(34) Lineweaver, H.; Burk, D. *J. Am. Chem. Soc.* **1934**, *56*, 658−666.
(35) Camplisson, C. K.; Schilling, K. M.; Pedrotti, W. L.; Stone, H. A.; Martinez, A. W. *Lab Chip* **2015**, *15*, 4461−4466.
(36) Fu, E.; Ramsey, S.; Kauffman, P.; Lutz, B.; Yager, P. *Microfluid. Nanofluid.* **2011**, *10*, 29−35.
(37) Lee, J.-H.; Chang, C.-K.; Park, J. In *International Conference on Miniaturized Systems for Chemistry and Life Sciences*; RSC Publishing: Gyeongju, KOREA, 2015; pp 1338−1340.
(38) Xiao, J.; Stone, H. A.; Attinger, D. *Langmuir* **2012**, *28*, 4208−4212.
(39) Yan, X.; Ge, X.; Cui, S. *Nanoscale Res. Lett.* **2011**, *6*, 313−313.
(40) Pasta, M.; La Mantia, F.; Cui, Y. *Electrochim. Acta* **2010**, *55*, 5561−5568.
(41) Hemalatha, T.; UmaMaheswari, T.; Krithiga, G.; Sankaranarayanan, P.; Puvanakrishnan, R. *Indian J. Exp. Biol.* **2013**, *51*, 777−788.
(42) Lequin, R. M. *Clin. Chem.* **2005**, *51*, 2415−2418.
(43) Gallagher, S. R. *GUS protocols: using the GUS gene as a reporter of gene expression*; Academic Press: New York, 2012.
(44) Batt, C. A. *Encyclopedia of Food Microbiology*, 2nd ed.; Academic Press: Oxford, 2014.
(45) Husain, Q. *Crit. Rev. Biotechnol.* **2010**, *30*, 41−62.
(46) Tang, H. T.; Lunte, C. E.; Halsall, H. B.; Heineman, W. R. *Anal. Chim. Acta* **1988**, *214*, 187−195.
(47) Johnson, K. A.; Goody, R. S. *Biochemistry* **2011**, *50*, 8264−8269.
(48) Laczka, O.; Ferraz, R. M.; Ferrer-Miralles, N.; Villaverde, A.; Muñoz, F. X.; Campo, F. J. d. *Anal. Chim. Acta* **2009**, *641*, 1−6.
(49) Viratelle, O. M.; Yon, J. M. *Eur. J. Biochem.* **1973**, *33*, 110−116.
(50) Sinawang, P. D.; Rai, V.; Ionescu, R. E.; Marks, R. S. *Biosens. Bioelectron.* **2016**, *77*, 400−408.
(51) Yamaguchi, M.; Matsuda, Y.; Sasaki, S.; Sasaki, M.; Kadoma, Y.; Imai, Y.; Niwa, D.; Shetty, V. *Biosens. Bioelectron.* **2013**, *41*, 186−191.
(52) Akanda, M. R.; Joung, H.-A.; Tamilavan, V.; Park, S.; Kim, S.; Hyun, M. H.; Kim, M.-G.; Yang, H. *Analyst* **2014**, *139* (6), 1420−1425.
(53) Bhimji, A.; Zaragoza, A. A.; Live, L. S.; Kelley, S. O. *Anal. Chem.* **2013**, *85* (14), 6813−6819.

DOI: 10.1021/acs.analchem.6b03010
Anal. Chem. 2016, 88, 10639−10647